Free energy of hydration and heat capacity of calcium dipicolinate in Bacillus spore cores

Ankit Mishra, Aravind Krishnamoorthy, Pankaj Rajak, Subodh Tiwari, Chunyang Sheng, Rajiv K. Kalia, Aiichiro Nakano, and Priya Vashishta

Citation: Appl. Phys. Lett. **113**, 113702 (2018); doi: 10.1063/1.5048507
View online: https://doi.org/10.1063/1.5048507
View Table of Contents: http://aip.scitation.org/toc/apl/113/11
Published by the American Institute of Physics

Free energy of hydration and heat capacity of calcium dipicolinate in *Bacillus* spore cores

Ankit Mishra, Aravind Krishnamoorthy, Pankaj Rajak, Subodh Tiwari, Chunyang Sheng, Rajiv K. Kalia, Aiichiro Nakano, and Priya Vashishta[a)]
Collaboratory for Advanced Computing and Simulations, University of Southern California, Los Angeles, California 90089, USA

(Received 15 July 2018; accepted 29 August 2018; published online 12 September 2018)

Wet heat treatments are widely used sterilization techniques for inactivating dangerous and resistant sporulating bacteria. The effectiveness of such treatments depends upon the thermodynamics of water uptake by the spore as well as the kinetics of phase transformations in the hydrated spore core. The mechanism behind these chemical and physical processes remains unknown because the thermodynamic properties of the spore core constituents are not well understood. Here, we use reactive molecular dynamics simulations to calculate the vibrational density of states and specific heat of hydrated calcium dipicolinate as well as the free energy of hydration based on Jarzynski's inequality. These two quantities are used to construct a phase diagram of hydrated calcium dipicolinate, indicating the extent of hydration at different pressures and temperatures, which can be used to identify potential regimes for wet-heat sterilization of bacterial spores.
https://doi.org/10.1063/1.5048507

Sporulation is a common defense mechanism in several bacterial species in response to low nutrient levels and adverse thermal, mechanical, and chemical environments.[1,2] The extraordinary resilience of bacterial spores permits them to overcome severe physical and chemical stresses and persist in a state of dormancy for extended periods of time ranging from a few days to millions of years.[3,4] This process of sporulation and subsequent re-germination of bacteria after exposure to sub-lethal stresses is of intense interest for strategic applications in the defense industry and of considerable commercial interest to the food preparation and preservation industries.[5] Wet-heat treatments like boiling, steaming, and autoclaving are the most commonly employed strategies to inactivate bacterial spores and prevent their re-germination. These sterilization techniques rely on the interplay of high temperature and increased water content in the cores of bacterial spores which contain metabolic enzymes, proteins, genetic materials, and salts of dipicolinic acid (DPA) with a divalent cation such as Ca^{2+}, Mg^{2+}, and Mn^{2+}.[6–9] Among these, DPA chelated with the Ca^{2+} cation to form calcium dipicolinate (Ca-DPA) is considered to be mechanistically important for the dormancy, heat resistance, and germination of spores.[10–14] Specifically, experiments involving chemical assays, attenuated total reflection Fourier transform infrared spectroscopy, and laser tweezers Raman spectroscopy[15,16] have identified the presence of Ca-DPA in the spore core matrix as being responsible for the dormancy of the spore core. Further, there is a correlation between the release of Ca-DPA from the spore core and subsequent spore death due to exposure to high pressure, temperature, wet-heat, and chemical agents.[13,17,18]

It has been hypothesized that the heat resistance of spores arises from suppressed enzymatic activity and protein agglomeration resulting from decreased diffusivity of the spore core matrix containing Ca-DPA in a glassy phase.[19] This is supported by a recent computational study which showed that environmental conditions corresponding to spore death coincide with conditions where the spore core is in a gel-like or molten phase.[20] The extent of spore-core hydration was found to be a critical parameter that controls the temperature for the onset of solid-molten phase transformation and is therefore important for the wet-heat death of spores. The extent of hydration depends on the thermodynamics of water uptake, which is difficult to characterize experimentally.

In this paper, we use reactive molecular dynamics (RMD) simulations to calculate thermodynamic properties relevant to the wet-heat treatment process such as the free energy of Ca-DPA hydration and the heat capacity of the hydrated Ca-DPA crystal. Various approaches have been used for accelerated sampling and mapping of free energy landscape using molecular simulations.[21] The free energies of hydration, computed here using a non-equilibrium calculation methodology, show monotonically increasing behavior with increasing hydration of the Ca-DPA in the spore core. However, the specific heat capacity contribution of added water to Ca-DPA decreases with hydration. These two thermodynamic properties are used to construct a phase diagram of the spore core showing the extent of hydration at different pressures and temperatures, which can be used to identify potential regimes for wet-heat sterilization.

We use RMD simulations based on first-principles derived reactive force field (ReaxFF)[22–24] to calculate the specific heat and free energy of hydration of the Ca-DPA crystal. For notational brevity, Ca-DPA implies the [Ca-DPA.$3H_2O$]$_4$ crystal. This force field was developed to reproduce physical properties like lattice constants of the

a)Author to whom correspondence should be addressed: priyav@usc.edu

$[Ca\text{-}DPA.3H_2O]_4$ crystal.[20] Figure 1 shows the unit cell of the Ca-DPA crystal containing four Ca^{2+} ions and four DPA molecules along with twelve water molecules that are bound to Ca^{2+} ions. The crystal structure of the native form of calcium dipicolinate, $[Ca\text{-}DPA.3H_2O]_4$, which is found in the core of unhydrated spores, contains two types of H_2O molecules that differ in the number of calcium ions in their coordination shell.[25] We refer to H_2O molecules coordinated to one and two calcium ions as H_2O^1 and H_2O^2, respectively. Addition of excess water molecules increases the level of hydration of the Ca-DPA crystal, leading to the formation of $[Ca\text{-}DPA{\cdot}3H_2O]_4 + nH_2O$—where n defines the number of added water molecules per unit cell. We refer to the added excess water molecules as H_2O^0 to denote that they are not bonded to any of the Ca^{2+} ions in the Ca-DPA crystal. These unbound water molecules occupy interstitial spaces within the crystal. We refer to the oxygen atoms in the H_2O^1, H_2O^2, and H_2O^0 as O^1, O^2, and O^0, respectively. Oxygen atoms that are part of the Ca-DPA molecule (i.e., do not belong to a water molecule) are denoted as O^{DPA}.

Hydrated Ca-DPA systems (containing 23.50, 25.99, 29.43, 31.55, and 33.54 wt. % water) are prepared by adding 2, 4, 7, 9, and 11 water molecules, respectively, per unit cell to the Ca-DPA crystal that already contains 12 bound water molecules. Zero-pressure configurations of these systems are obtained by first adding the corresponding number of excess water molecules to the $[Ca\text{-}DPA.3H_2O]_4$ unit cells, which are then expanded in volume and thermalized to obtain zero-pressure states at room temperature. These thermalized systems are discussed in detail in the supplementary material and serve as initial configurations for the calculation of both the heat capacity and the free energy of hydration as described in subsequent paragraphs.

The zero pressure configurations obtained at a temperature of 300 K with $n = 0$, 2, 4, 7, 9, and 11 waters in $[Ca\text{-}DPA{\cdot}3H_2O]_4 + nH_2O$ are slowly cooled to 100 K in steps of 50 K. The velocity information from a 6 ps long RMD trajectory in the NVE ensemble is used to calculate normalized velocity auto correlation functions (VACF) for various species (C, H, O, N, and Ca atoms of Ca-DPA and H and O atoms of H_2O^0, H_2O^1, and H_2O^2) using the following equation:

$$Z_\alpha = \frac{\langle \vec{v}_{i\alpha}(0).\vec{v}_{i\alpha}(t)\rangle}{\langle \vec{v}_{i\alpha}(0).\vec{v}_{i\alpha}(0)\rangle}. \tag{1}$$

In the above equation, Z_α is the VACF for species α, and $v_{i\alpha}(t)$ is the velocity of the i^{th} atom of species α at time t and brackets denote the average over atom and time origins. From the VACF, we calculate the partial vibrational density of states[26] (pDOS), $G_\alpha(\omega)$, for the different species mentioned above using Eq. (2). The total vibrational density of states, $G(\omega)$, of the Ca-DPA crystal is a sum of the pDOS for different species [Eq. (3)]

$$G_\alpha(\omega) = \frac{6N_\alpha}{\pi}\int_0^\infty Z_\alpha(t)\cos(\omega t)dt, \tag{2}$$

$$G(\omega) = \sum_\alpha G_\alpha(\omega). \tag{3}$$

Density of states is calculated at a relatively low temperature of 100 K in order to preclude any long-range diffusion of added water which could affect the calculation of velocity autocorrelation functions. The total density of states for two representative hydrations, $n = 0$, 11 (i.e., $[Ca\text{-}DPA.3H_2O]_4$ and $[Ca\text{-}DPA.3H_2O]_4 + 11\ H_2O$), is shown in Fig. 2. Vibrational density of states for other hydration values is plotted in the supplementary material. The main features of the calculated vibrational density of states in Fig. 2(a) are in qualitative agreement with the experimental Raman and IR spectra of the $[Ca\text{-}DPA.3H_2O]_4$.[8,9] A comparison of Figs. 2(a) and 2(b) indicates that the main difference between the vibrational density of states of the hydrated and unhydrated Ca-DPA arises from the contribution of 11 excess water molecules.

Using the pDOS calculated above in Eqs. (2) and (3), we calculate partial heat capacities (at constant volume) per mole of each atomic species, α, present in $[Ca\text{-}DPA.3H_2O]_4 + nH_2O$. The specific heat of different molecules like Ca-DPA, H_2O^2, and H_2O^0 can be computed as the stoichiometric sum of the partial heat capacities of component atomic species

$$C_v = \frac{3Nk_B\int_0^\infty \frac{u^2e^u}{(e^u-1)^2}G(\omega)d\omega}{\int_0^\infty G(\omega)d\omega}, \tag{4}$$

where $u = \hbar\omega/k_BT$ and k_B is the Boltzmann constant.

The computed heat capacity values for different constituents of the $[Ca\text{-}DPA.3H_2O]_4 + nH_2O$ system are shown in Fig. 3. The heat capacities of the Ca-DPA molecule and the (singly and doubly) bonded water molecules are higher in the hydrated system at all temperatures, reflecting the relatively weak bonding of excess water molecules.

Figure 4 shows the average heat capacity per water molecule in the hydrated Ca-DPA as a function of water content. The heat capacity decreases monotonically from 36 J mol^{-1} K^{-1} in $[Ca\text{-}DPA.3H_2O]_4 + 2H_2O$ to 32 J mol^{-1} K^{-1} in $[Ca\text{-}DPA.3H_2O]_4 + 11\ H_2O$, approximately equal to that of bulk water in ice-Ih,[27] suggesting that water uptake detrimentally affects the heat resistance of spore cores.

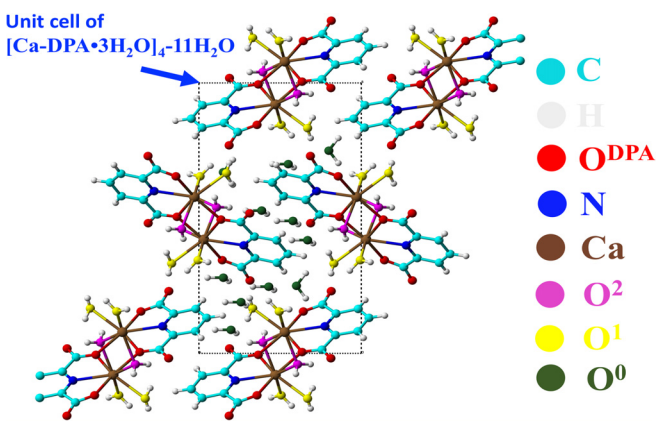

FIG. 1. $[Ca\text{-}DPA.3H_2O]_4 + 11\ H_2O$ configuration corresponding to addition of 11 additional water to the unit cell (black) with a water content of 33.54 wt. % H_2O. The oxygen atoms corresponding to singly (O^1) and doubly (O^2) coordinated water molecules with calcium of Ca-DPA are highlighted in yellow and magenta, respectively. The oxygen atom of added water O^0 is highlighted in green.

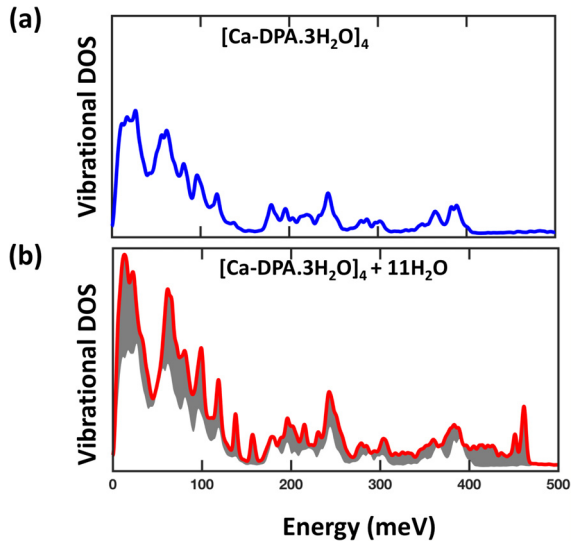

FIG. 2. Total vibrational density of states for (a) $[Ca\text{-}DPA.3H_2O]_4$ and (b) $[Ca\text{-}DPA.3H_2O]_4$ +11 H_2O (33.54 wt. % water) systems. The difference between the DOS profiles, shown in gray in (b), is due to contributions from the addition of water.

Another important thermodynamic metric for the hydration process is the free energy of hydration, which quantifies the susceptibility of the spore core to undergo hydration (i.e., absorption of water molecules from the environment) or dehydration (i.e., release of water molecules from the hydrated spore core) under given P-T conditions. Hydration free energy was calculated using Jarzynski's method[28–30] [Eq. (5)], which relates the free energy difference between two systems, ΔF, to the ensemble average of the work done, W, along a finite MD trajectory connecting the two systems

$$\Delta F = -k_B T \times \ln\left\langle e^{-\frac{W}{k_B T}}\right\rangle. \tag{5}$$

The work done during the addition of water molecules to the Ca-DPA crystal is calculated as follows. Addition of water

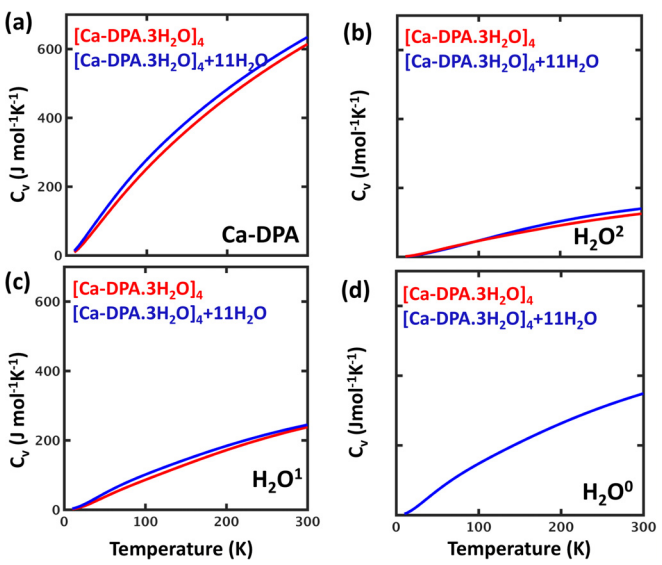

FIG. 3. Partial heat capacities of (a) Ca-DPA, (b) H_2O^1, (c) H_2O^2, and (d) H_2O^0. The red curves are computed per mole of un-hydrated $[Ca\text{-}DPA.3H_2O]_4$ crystal that has Ca-DPA, H_2O^1, and H_2O^2. Blue curves are computed per mole of the hydrated $[Ca\text{-}DPA.3H_2O]_4$ + $11H_2O$ system where H_2O^0 is added. Contributions of Ca-DPA, H_2O^1, and H_2O^2 increase slightly upon hydration, but the main difference arises from excess added water H_2O^0.

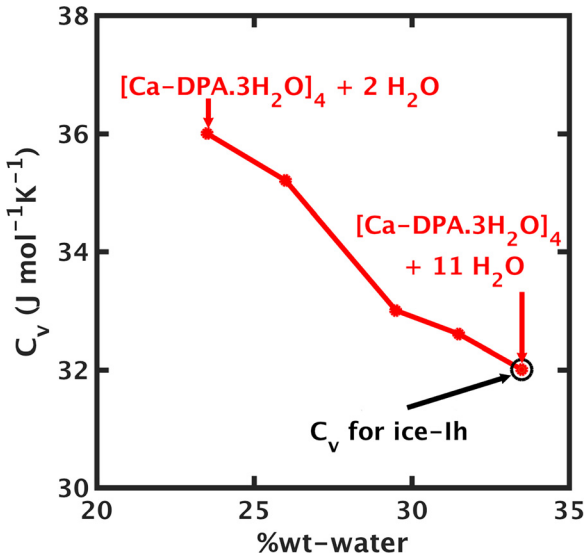

FIG. 4. Specific heat per mole of added excess water in $[Ca\text{-}DPA.3H_2O]_4 + nH_2O$ as a function of total water content.

to the zero-pressure $[Ca\text{-}DPA.3H_2O]_4$ crystal at constant volume to form $[Ca\text{-}DPA.3H_2O]_4 + nH_2O$ leads to an increase in pressure to a value of P_{start}. This system is expanded in incremental steps of ΔV and thermalized at this volume to obtain several intermediate values of pressure $P_{int} < P_{start}$. This volume expansion process is continued until the system pressure reduces to the initial value of $P_{ref} = 0$ GPa. The area under the P-V curve so constructed defines the non-equilibrium work W, performed during hydration of the $[Ca\text{-}DPA.3H_2O]_4$ crystal at constant volume, as shown in Fig. 5.

Based on the calculation methodology discussed above, we compute P-V curves for Ca-DPA systems at different levels of hydration corresponding to temperatures between 273 K and 368 K. The P-V curve for 300 K is shown in Fig. 6. P–V curves at different temperatures for systems with $n = 2$, 4, 7, and 9 added water are reported in the supplementary material. The calculated free energy of hydration increases with increasing hydration and decreases with increasing temperature for a given value of hydration, within the temperature range considered here (273 K–368 K).

The specific heat and free energy of hydration are used to estimate $\Delta\mu$, the difference in chemical potential of water molecules in the Ca-DPA matrix and in bulk liquid water at a constant temperature and pressure. A positive value of $\Delta\mu$ indicates that water molecules flow from the bulk liquid water into the Ca-DPA matrix leading to hydration of the spore core. Conversely, a negative value of $\Delta\mu$ indicates that water preferentially leaves the Ca-DPA matrix for the bulk liquid water phase leading to spore dehydration. We estimate the difference in water chemical potential using the following equation:

$$\Delta\mu(T,P) = \Delta\Omega(300\,\mathrm{K}) + \mathrm{T}\int_{300K}^{T}\frac{\Delta C_V}{T}\,\mathrm{dT}, \tag{6}$$

where $\Delta\mu(T,P)$ is the calculated difference in chemical potential, and $\Delta\Omega$ is the difference in grand canonical free energy; $\Omega = -PV$ of water molecules, given by $\Delta\Omega = P \cdot \left[V_{wat}(P) - V_{DPA}(P)\right]$. $V_{wat}(P)$ and $V_{DPA}(P)$ are the

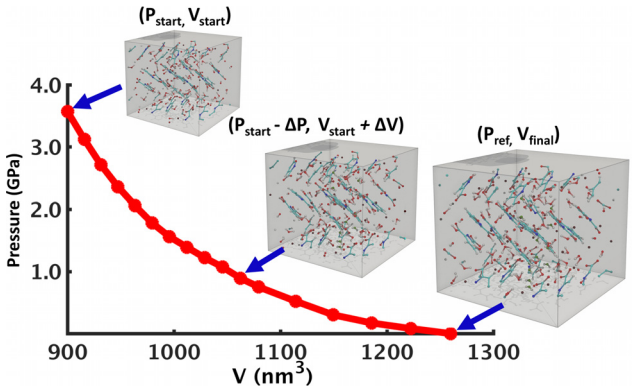

FIG. 5. Procedure for calculating of free energy of the $[Ca\text{-}DPA.3H_2O]_4 + 11\ H_2O$ system at 300 K. The addition of excess water leads to pressure value P_{start} at a given temperature. This system is expanded in steps of ΔV to reach an intermediate step having lower pressure value $P_{int} < P_{start}$. Successive expansions bring the system to the same pressure (P_{ref}) as that of the reference $[Ca\text{-}DPA.3H_2O]_4$ system. The trajectory so obtained is used to compute hydration free energy of at constant volume.

partial molar volumes of water molecules in the bulk water molecules and Ca-DPA phases at pressure P, respectively, as obtained from the respective P–V curves. The P–V curve for the bulk water system is calculated following the methodology for hydrated Ca-DPA systems as shown in the supplementary material. The difference in the molar heat capacity of water (ΔC_V) in hydrated Ca-DPA and bulk water is obtained from the calculated vibrational density of states of the respective systems. Equation (6) defines the difference between chemical potential of water molecules in the Ca-DPA matrix and liquid water. The free energy difference between water molecules in hydrated Ca-DPA and the water vapor phase can be obtained by including an additional term corresponding to the difference between free energies of liquid water and steam at a given temperature and pressure [Eq. (7)]

$$\Delta\mu(T,P) = \Delta\Omega(300\,\mathrm{K}) + T\int_{300\mathrm{K}}^{T}\frac{\Delta C_V}{T}\,dT + k_B\,T\ln\frac{P}{P_{vap}(T)}, \tag{7}$$

where $P_{vap}(T)$ is the vapor pressure of H_2O at T Kelvin.

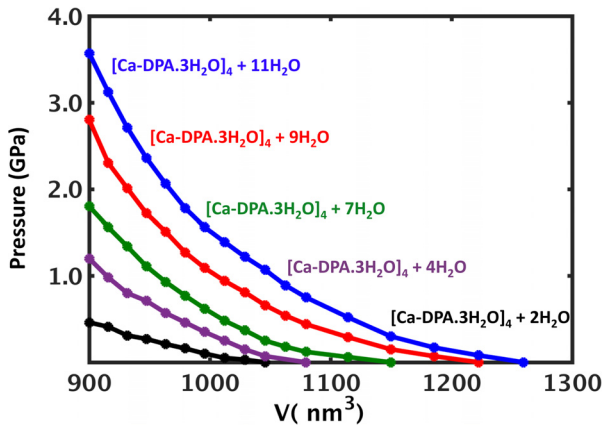

FIG. 6. Calculated P-V curves for $[Ca\text{-}DPA.3H_2O]_4 + nH_2O$; n = 2, 4, 7, 9, and 11 at T = 300 K obtained following the schematic discussed in Fig. 5.

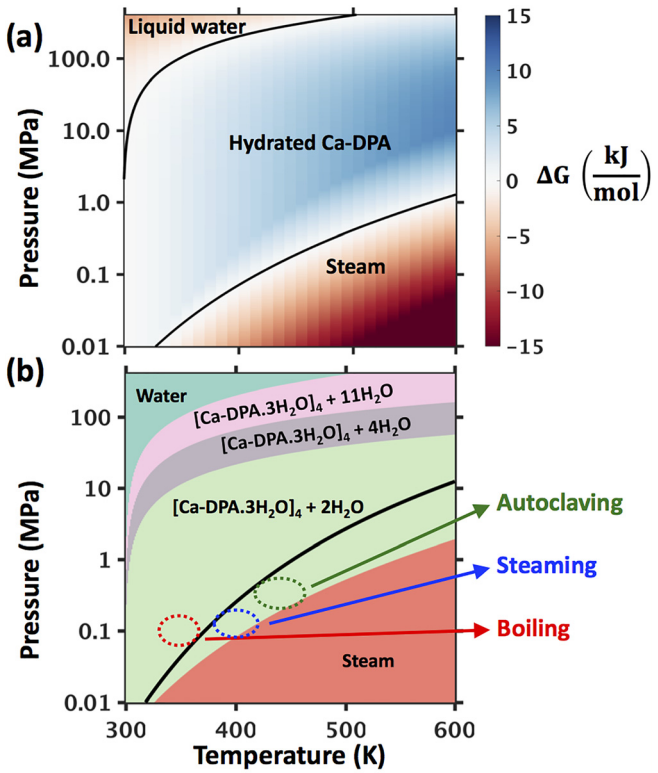

FIG. 7. (a) Free energy difference of water and hydrated Ca-DPA for different temperatures and pressures has distinct regions of hydration and dehydration. (b) Regions of stability correspond to various hydrations in Ca-DPA. The solid black line is the liquid-vapor boundary of water.

We use Eqs. (6) and (7) to estimate $\Delta\mu$ at temperatures between 300 K and 600 K and pressure values in the range of 0.01 MPa–400 MPa [Fig. 7(a)]. The value of $\Delta\mu(T,P)$ defines three distinct regions in the T-P space. High temperature and low-pressure regions are characterized by negative values of $\Delta\mu$ and correspond to physical conditions where water molecules evaporate from hydrated Ca-DPA leading to spore dehydration. At high pressures and low temperatures, the chemical potential of water in the high-density bulk liquid phase is lower than in the low-density Ca-DPA matrix which leads to dehydration. In contrast, regions of intermediate temperature and pressure, particularly close to the ambient pressure ($P = 0.1$ MPa) and boiling point of water ($T = 373$ K), have positive $\Delta\mu$ values indicating the stability of the hydrated Ca-DPA.

The calculation of heat capacity and free energy of hydration for $[Ca\text{-}DPA.3H_2O]_4 + nH_2O$; $n = 0$, 2, 4, 7, 9, and 11 allows us to estimate the relative stabilities of Ca-DPA phases with different levels of hydration as a function of temperature and pressure. Figure 7(b) shows the phase diagrams of the most stable $[Ca\text{-}DPA.3H_2O]_4 + nH_2O$ and bulk water phases. Regimes corresponding to wet-heat treatments like boiling, steaming, and autoclaving lie within the stability domain of partially hydrated Ca-DPA. Figure 7(b) also suggests that other temperature and pressure conditions, like high-pressure boiling ($T = 373$ K and $P > 0.1$ MPa), could be viable alternatives for spore death.

In conclusion, we have used reactive molecular dynamics simulations to calculate vibrational density of states and non-equilibrium quasi-static P–V work to evaluate the heat

capacity and hydration free energy of hydrated Ca-DPA crystals. These values are used to construct a phase diagram of the hydrated spore core to identify regimes of temperature and pressure where hydration (or dehydration) of the spore core is thermodynamically favorable. The stability regimes identified in the phase diagram are in agreement with commonly used wet-heat treatments and also suggest new pressure and temperature conditions for spore sterilization.

See supplementary material for the system set up and simulation details.

This research was supported by the Defense Threat Reduction Agency Grant No. HDTRA1-14-1-0074. We thank Dr. Douglas Allen Dalton and Dr. Suhithi Peiris for their encouragement and continued support throughout this investigation.

[1]D. W. Hilbert and P. J. Piggot, Microbiol. Mol. Biol. Rev. **68**, 234 (2004).
[2]P. Stragier and R. Losick, Annu. Rev. Genet. **30**, 297 (1996).
[3]R. Kort, A. C. O'Brien, I. H. M. Stokkum, S. J. C. M. Oomes, W. Crielaard, K. J. Hellingwerf, and S. Brul, Appl. Environ. Microbiol. **71**, 3556 (2005).
[4]R. H. Vreeland, W. D. Rosenzweig, and D. W. Powers, Nature **407**, 897 (2000).
[5]S. R. B. R. Sella, L. P. S. Vandenberghe, and C. R. Soccol, Microbiol. Res. **169**, 931 (2014).
[6]B. Setlow, S. Atluri, R. Kitchel, K. K. Dube, and P. Setlow, J. Bacteriol. **188**, 3740 (2006).
[7]A. C. Granger, E. K. Gaidamakova, V. Y. Matrosova, M. J. Daly, and P. Setlow, Appl. Environ. Microbiol. **77**, 32 (2011).
[8]P. Carmona, Spectrochim. Acta, Part A **36**, 705 (1980).
[9]K. McCann and J. Laane, J. Mol. Struct. **890**, 346 (2008).
[10]I. R. Scott and D. J. Ellar, J. Bacteriol. **135**, 133 (1978).
[11]P. Setlow, Curr. Opin. Microbiol. **6**, 550 (2003).
[12]P. Setlow, J. Appl. Microbiol. **101**, 514 (2006).
[13]M. Paul, S. Atluri, B. Setlow, and P. Setlow, J. Appl. Microbiol. **101**, 1161 (2006).
[14]H. Shibata, S. Yamashita, M. Ohe, and I. Tani, Microbiol. Immunol. **30**, 307 (1986).
[15]H. Cheung, J. Cui, and S. Sun, Microbiology **145**, 1043 (1999).
[16]D. Chen, S. Huang, and Y. Q. Li, Anal. Chem. **78**, 6936 (2006).
[17]H. V. B. Veen, H. Xie, E. Esveld, T. Abee, H. Matswijk, and M. N. Groot, Food Microbiol. **45**, 26 (2015).
[18]C. J. Doona, F. E. Feeherry, B. Setlow, W. Shiwei, L. William, F. C. Nichols, P. K. Talukdar, M. R. Sarker, Y. Q. Li, S. Aimee, and P. Setlow, Appl. Environ. Microbiol. **82**, 5287 (2016).
[19]E. P. Sunde, P. Setlow, L. Hederstedt, and B. Halle, Proc. Natl. Acad. Sci. U. S. A. **106**, 19334 (2009).
[20]P. Rajak, A. Mishra, C. Sheng, S. Tiwari, A. Krishnamoorthy, R. K. Kalia, A. Nakano, and P. Vashishta, Appl. Phys. Lett. **111**, 213701 (2017).
[21]J. Henin, G. Fiorin, C. Chipot, and M. Klein, J. Chem. Theory Comput. **6**, 35 (2010).
[22]A. C. T. van Duin, S. Dasgupta, F. Lorant, and W. A. Goddard, J. Phys. Chem. A **105**, 9396 (2001).
[23]K.-I. Nomura, P. E. Small, R. K. Kalia, A. Nakano, and P. Vashishta, Comput. Phys. Commun. **192**, 91 (2015).
[24]J. M. D. Lane, G. S. Grest, A. P. Thompson, K. R. Cochrane, M. Desjarlais, and T. R. Mattsson, AIP Conf. Proc. **1426**, 1435 (2012).
[25]G. Strahs and R. E. Dickerson, Acta Crystallogr. B **24**, 571 (1968).
[26]D. D. Dlott, Annu. Rev. Phys. Chem. **37**, 157 (1986).
[27]E. C. Spencer, A. A. Levchenko, N. L. Ross, A. I. Kolesnikov, J. B. Goates, B. F. Woodfield, A. Navrotsky, and G. Li, J. Phys. Chem. A **113**, 2796 (2009).
[28]C. Jarzynski, Phys. Rev. Lett. **78**, 2690 (1997).
[29]C. Jarzynski, Phys. Rev. E **56**, 5018 (1997).
[30]C. Jarzynski, J. Stat. Mech. **1**, P09005 (2004).